Astron. Astrophys. 362, 295–309 (2000)

ASTRONOMY AND ASTROPHYSICS

New theoretical mass-loss rates of O and B stars

J.S. Vink[1], **A. de Koter**[2], **and H.J.G.L.M. Lamers**[1,3]

[1] Astronomical Institute, Utrecht University, P.O. Box 80000, 3508 TA Utrecht, The Netherlands
[2] Astronomical Institute "Anton Pannekoek", University of Amsterdam, Kruislaan 403, 1098 SJ Amsterdam, The Netherlands
[3] SRON Laboratory for Space Research, Sorbonnelaan 2, 3584 CA Utrecht, The Netherlands

Received 14 February 2000 / Accepted 7 August 2000

Abstract. We have calculated mass-loss rates for a grid of wind models covering a wide range of stellar parameters and have derived a mass-loss recipe for two ranges of effective temperature at either side of the bi-stability jump around spectral type B1.

For a large sample of O stars, it is shown that there is now good agreement between these new theoretical mass-loss rates that take *multiple scattering* into account and observations.

Agreement between the observed and new theoretical wind momenta increases confidence in the possibility to derive distances to luminous stars in distant stellar systems using the Wind momentum Luminosity Relation.

For the winds of the B stars there is an inconsistency in the literature between various mass-loss rate determinations from observations by different methods. One group of $\dot{M}$ determinations of B stars *does* follow the new theoretical relation, while another group does not. The lack of agreement between the observed mass-loss rates derived by different methods may point to systematic errors in mass-loss determinations from observations for B stars.

We show that our theoretical mass-loss recipe is reliable and recommend it be used in evolutionary calculations.

Key words: stars: early-type – stars: mass-loss – stars: supergiants – stars: winds, outflows – stars: evolution

1. Introduction

In this paper we present new theoretical mass-loss rates $\dot{M}$ for a wide range of parameters for galactic O and B stars, taking *multiple scattering* into account. These predictions for $\dot{M}$ are compared with observations. The goal of the paper is to derive an accurate description of mass loss as a function of stellar parameters.

Early-type stars have high mass-loss rates, which substantially affects their evolution (e.g. Chiosi & Maeder 1986). The winds of early-type stars are most likely driven by radiation pressure in lines and in the continuum. The radiation-driven wind theory was first developed by Lucy & Solomon (1970) and Castor et al. (1975) (hereafter CAK). At a later stage the theory was improved by Abbott (1982), Friend & Abbott (1986), Pauldrach et al. (1986) and Kudritzki et al. (1989).

During the last decade, the radiation-driven wind theory has been compared with the most reliable mass-loss determinations from observations that are available: mass loss determined from radio data and from the analysis of Hα line profiles. Both Lamers & Leitherer (1993) and Puls et al. (1996) came to the conclusion that the theory of radiation-driven winds shows a *systematic discrepancy* with the observations. For O stars the radiation-driven wind theory predicts systematically *lower* values for mass loss than have been derived from observations.

Since the discrepancy increases as a function of wind density, it is possible that the reason for this is an inadequate treatment of "multiple scattering" in the current state of radiation-driven wind theory. It has been suggested (e.g. by Lamers & Leitherer 1993) that the "momentum-problem" that has been observed in the dense winds of Wolf-Rayet stars is the more extreme appearance of this discrepancy seen in the winds of normal O-type stars.

Because the observed mass-loss rates for O type supergiants are typically a factor of two higher than the values predicted by radiation-driven wind theory, evolutionary models would be significantly affected if theoretical values were adopted. It is obvious that an accurate description of mass loss is of great importance to construct reliable evolutionary tracks for massive stars.

Abbott & Lucy (1985) and Puls (1987) have investigated the importance of "multiple scattering" relative to "single scattering" for the winds of O stars. Abbott & Lucy found an increase in $\dot{M}$ of a factor of about three for the wind of the O supergiant ζ Puppis if multiple scattering was applied in a Monte Carlo simulation.

We will use a similar Monte Carlo technique in which multiple scatterings are taken into account to calculate mass-loss rates for a wide range of stellar parameters throughout the upper part of the Hertzsprung-Russell Diagram (HRD). In Sect. 2, the approach to calculate mass-loss rates will be briefly described, while in Sect. 3, a grid of wind models and mass-loss rates will be presented. A clear separation of the HRD into two parts will be made. The first range is that on the "hot" side of the *bi-stability* jump near spectral type B1, where the ratio of the terminal velocity to the effective escape velocity at the

Send offprint requests to: J.S. Vink (j.s.vink@astro.uu.nl)

stellar surface ($v_\infty/v_{\rm esc}$) is about 2.6; the second range is that on the "cool" side of the jump where the ratio suddenly drops to about 1.3 (Lamers et al. 1995). At the jump the mass-loss rate is predicted to change dramatically due to a drastic change in the ionization of the wind (Vink et al. 1999). In Sect. 4, the theoretical wind momentum will be studied and in Sect. 5 fitting formulae for the mass-loss rate will be derived by means of multiple linear regression methods: this yields a recipe to predict $\dot{M}$ as a function of stellar parameters. In Sect. 6 these predicted mass-loss rates will be compared with observational rates. *We will show that for O stars theory and observations agree if "multiple scattering" is properly taken into account.* Finally, in Sects. 7 and 8 the study will be discussed and summarized.

2. Method to calculate $\dot{M}$

The basic physical properties of the adopted Monte Carlo (MC) method to predict mass-loss rates are similar to the technique introduced by Abbott & Lucy (1985). The precise method was extensively described in Vink et al. (1999). The core of the approach is that the total loss of radiative energy is linked to the total gain of momentum of the outflowing material. The momentum deposition in the wind is calculated by following the fate of a large number of photons that are released from below the photosphere.

The calculation of mass loss by this method requires the input of a model atmosphere, before the radiative acceleration and $\dot{M}$ can be calculated. The model atmospheres used for this study are calculated with the most recent version of the non-LTE unified[1] Improved Sobolev Approximation code (ISA-WIND) for stars with extended atmospheres. For details we refer the reader to de Koter et al. (1993,1997). The chemical species that are explicitly calculated in non-LTE are H, He, C, N, O and Si. The iron-group elements, which are important for the radiative acceleration and $\dot{M}$, are treated in the modified nebular approximation (see Schmutz 1991).

3. The predicted mass-loss rates

Using the procedure summarized in Sect. 2, we have calculated mass-loss rates for 12 values of $T_{\rm eff}$ in the range between 12 500 and 50 000 K. For every effective temperature a grid of 12 series of models for galactic stars was calculated with luminosities in the range log ($L_*/L_\odot$) = 4.5–6.25 and masses in the range M_* = 15–120 $M_\odot$. For these 144 models, mass-loss rates were calculated for three values of the ratio $v_\infty/v_{\rm esc}$, yielding a total number of 432 models.

The parameters for all series of models are indicated in Table 1. In Fig. 1 the luminosities and effective temperatures of the models are indicated with asterisks on top of evolutionary tracks to show the coverage of the model grid over the upper HRD. To study the mass-loss dependence on different stellar parameters (L, M and $T_{\rm eff}$) separately, a wide range of parameters was chosen, this implies that some of the models in Fig. 1 have positions to the *left* of the main sequence. We enumerate the assumptions in the model grid:

1. The models are calculated for solar metallicities (Allen 1973).
2. The stellar masses in the grid of models were chosen in such a way that they are representative for the evolutionary luminosities of the tracks from the Geneva group (Meynet et al. 1994). To investigate the dependence of $\dot{M}$ on M_*, a number of smaller and larger values for M_* was also chosen (see Column (3) in Table 1).
3. The grid was constructed in a way that $\Gamma_e \lesssim 0.5$ (see Column (4) in Table 1), where Γ_e is the ratio between the grav-

[1] ISA-WIND treats the photosphere and wind in a unified manner. This is distinct from the so-called "core-halo" approaches.

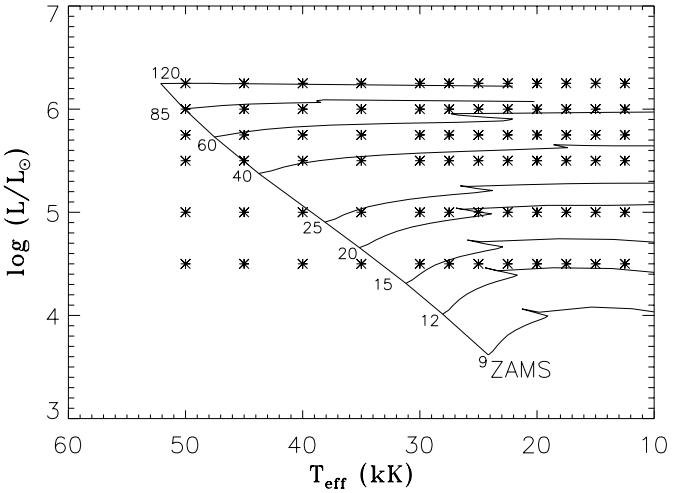

Fig. 1. Coverage of the calculated wind models over the HRD. The crosses indicate the model values of log $L/L_\odot$ and $T_{\rm eff}$. Evolutionary tracks from Meynet et al. (1994) are shown for several initial masses, which are indicated in the plot. The Zero Age Main Sequence (ZAMS) is also shown.

Table 1. Parameters for the 12 (L_*, M_*) series of wind models. For details about the model assumptions and grid spacing, see text.

series no	logL_* ($L_\odot$)	M_* ($M_\odot$)	$\Gamma_{\rm e}$	$M_{\rm eff}$ ($M_\odot$)	$T_{\rm eff}$ (kK)	$\left(\frac{v_\infty}{v_{\rm esc}}\right)$
1	4.5	15	0.055	14.2	12.5–50.0	1.3–2.6
2		20	0.041	19.2	12.5–50.0	1.3–2.6
3	5.0	20	0.130	17.4	12.5–50.0	1.3–2.6
4		30	0.087	27.4	12.5–50.0	1.3–2.6
5		40	0.068	37.3	12.5–50.0	1.3–2.6
6	5.5	30	0.274	21.8	12.5–50.0	1.3–2.6
7		40	0.206	31.8	12.5–50.0	1.3–2.6
8		50	0.165	41.8	12.5–50.0	1.3–2.6
9	5.75	45	0.325	30.4	12.5–50.0	1.3–2.6
10	6.0	60	0.434	34.0	12.5–50.0	1.3–2.6
11		80	0.326	53.9	12.5–50.0	1.3–2.6
12	6.25	120	0.386	73.7	12.5–50.0	1.3–2.6

itational acceleration and the radiative acceleration due to electron scattering. Γ_e is given by:

$$\Gamma_e \;=\; \frac{L\sigma_e}{4\pi cGM} \;=\; 7.66\,10^{-5}\sigma_e \left(\frac{L}{L_\odot}\right)\left(\frac{M}{M_\odot}\right)^{-1} \quad (1)$$

where σ_e is the electron scattering cross-section (its value is taken as determined in Lamers & Leitherer 1993) and the other constants have their usual meaning. For values of $\Gamma_e > 0.5$, the stars approach their Eddington limit and the winds show more dramatic mass-loss behaviour. In this study, stellar parameters for these "Luminous Blue Variable-like" stars are excluded to avoid confusion between various physical wind effects.

4. All series of models from Table 1 have effective temperatures between 12 500 and 50 000 K, with a stepsize of 2 500 K from 12 500 to 30 000 K and a stepsize of 5 000 K, starting from 30 000 up to 50 000 K.
5. We calculated $\dot{M}$ for wind models with a β-type velocity law for the accelerating part of the wind:

$$v(r) \;=\; v_\infty \left(1 \;-\; \frac{R_*}{r}\right)^{\beta} \quad (2)$$

Below the sonic point, a smooth transition from this velocity structure is made to a the velocity that follows from the photospheric density structure. A value of $\beta = 1$ was adopted in the accelerating part of the wind. This is a typical value for normal OB supergiants (see Groenewegen & Lamers 1989; Haser et al. 1995; Puls et al. 1996). At a later stage models for other β values will be calculated and it will be demonstrated that the predicted $\dot{M}$ is essentially insensitive to the adopted value of β (see Sect. 5.4).

6. The dependence of $\dot{M}$ on various values of v_∞ was determined. Lamers et al. (1995) found that the ratio $v_\infty/v_{\rm esc} \simeq 2.6$ for stars of types earlier than B1, and drops to $v_\infty/v_{\rm esc} \simeq 1.3$ for stars later than type B1. Therefore, we calculated mass-loss rates for various input values of this ratio, namely 1.3, 2.0 and 2.6 to investigate the mass loss as a function of this parameter, similar to that in Vink et al. (1999). For the determination of $v_{\rm esc}$, the effective mass $M_{\rm eff} = M_*(1-\Gamma_e)$ was used. $M_{\rm eff}$ is given in Column (5) of Table 1.

3.1. $\dot{M}$ for supergiants in Range 1 (30 000 $\leq T_{\rm eff} \leq$ 50 000 K)

The results for the complete grid of all the 12 (L_*, M_*) series are plotted in the individual panels of Fig. 2. Note that for *each* calculated point in the grid, *several* wind models had to be calculated to check which adopted mass-loss rate was consistent with the radiative acceleration (see Lucy & Abbott 1993). This yields predicted, self-consistent values for $\dot{M}$ (see Vink et al. 1999).

For each (L_*, M_*) set and for each value of $v_\infty/v_{\rm esc}$, we found that the mass loss decreases for decreasing effective temperature between 50 000 and 27 500 K. The reason for this fall-off is essentially that the maximum of the flux distribution gradually shifts to longer wavelengths. Since there are significantly less lines at roughly $\lambda \gtrsim 1800$ Å than at shorter wavelength, the line acceleration becomes less effective at lower $T_{\rm eff}$, and thus $\dot{M}$ decreases.

Table 2. Bi-stability jump characteristics for the 12 (L_*, M_*) series of wind models.

series no	log L_* ($L_\odot$)	M_* ($M_\odot$)	log($\Delta\dot{M}$)	$T_{\rm eff}^{\rm jump}$ (K)	$\langle\rho\rangle^{\rm jump}$ (g cm^{-3})
1	4.5	15	0.78	23 750	-14.82
2		20	0.61	22 500	-15.13
3	5.0	20	0.83	26 250	-14.22
4		30	0.87	25 000	-14.68
5		40	0.73	25 000	-14.74
6	5.5	30	0.76	26 250	-13.89
7		40	0.81	26 250	-14.13
8		50	0.82	25 000	-14.40
9	5.75	45	0.77	25 000	-13.93
10	6.0	60	0.76	25 000	-13.66
11		80	0.76	26 250	-13.89
12	6.25	120	0.77	25 000	-13.87

3.2. $\dot{M}$ at the bi-stability jump around 25 000 K

Between about $T_{\rm eff} = 27\,500$ and 22 500 K the situation is reversed: in this range the mass loss *increases* drastically with decreasing $T_{\rm eff}$. These increments in $\dot{M}$ coincide both in $T_{\rm eff}$ and in size of the $\dot{M}$ jump with the bi-stability jump that was studied by Vink et al. (1999). They showed that the origin of the jump is linked to a shift in the ionization balance of iron in the lower part of the wind and that it is this element that dominates the line driving at the base of the wind. Below $T_{\rm eff} \simeq 25\,000$ K, Fe IV recombines to Fe III and as this latter ion is a more efficient line driver than Fe IV, the line acceleration in the lower part of the wind increases. This results in an upward jump in $\dot{M}$ of about a factor of five and subsequently a drop in v_∞. The drop in v_∞ was predicted to be a factor of two, which is confirmed by determinations of v_∞ of OB supergiants from ultraviolet data by Lamers et al. (1995). A comparison between the spectral type of the *observed* bi-stability jump and the effective temperature of the *predicted* jump, was made in Vink et al. (1999).

Since we know from both theory and observations that the ratio $v_\infty/v_{\rm esc}$ jumps from ~ 2.6 at the hot side of the jump to ~ 1.3 at the cool side of the jump, we can predict the jump in mass loss for all 12 (L_*, M_*) series of models. The size of the jump is defined as the difference between the minimum $\dot{M}$ at the hot side of the jump (where $v_\infty/v_{\rm esc}$ = 2.6) and the maximum $\dot{M}$ at the cool side (where $v_\infty/v_{\rm esc}$ = 1.3) in Fig. 2. The size of the predicted jump in $\dot{M}$ (log $\Delta\dot{M}$) is indicated in Column (4) of Table 2: $\Delta\dot{M}$ is about a factor of five to seven. Table 2 tabulates additional characteristics for the models at the bi-stability jump.

The jump in mass loss around $T_{\rm eff} \simeq 25\,000$ K is not exactly the same for all series of models: the jump occurs at somewhat different effective temperatures. This is no surprise, since the ionization equilibrium does not only depend on temperature, but on density as well. A smaller value of the ratio $v_\infty/v_{\rm esc}$ leads

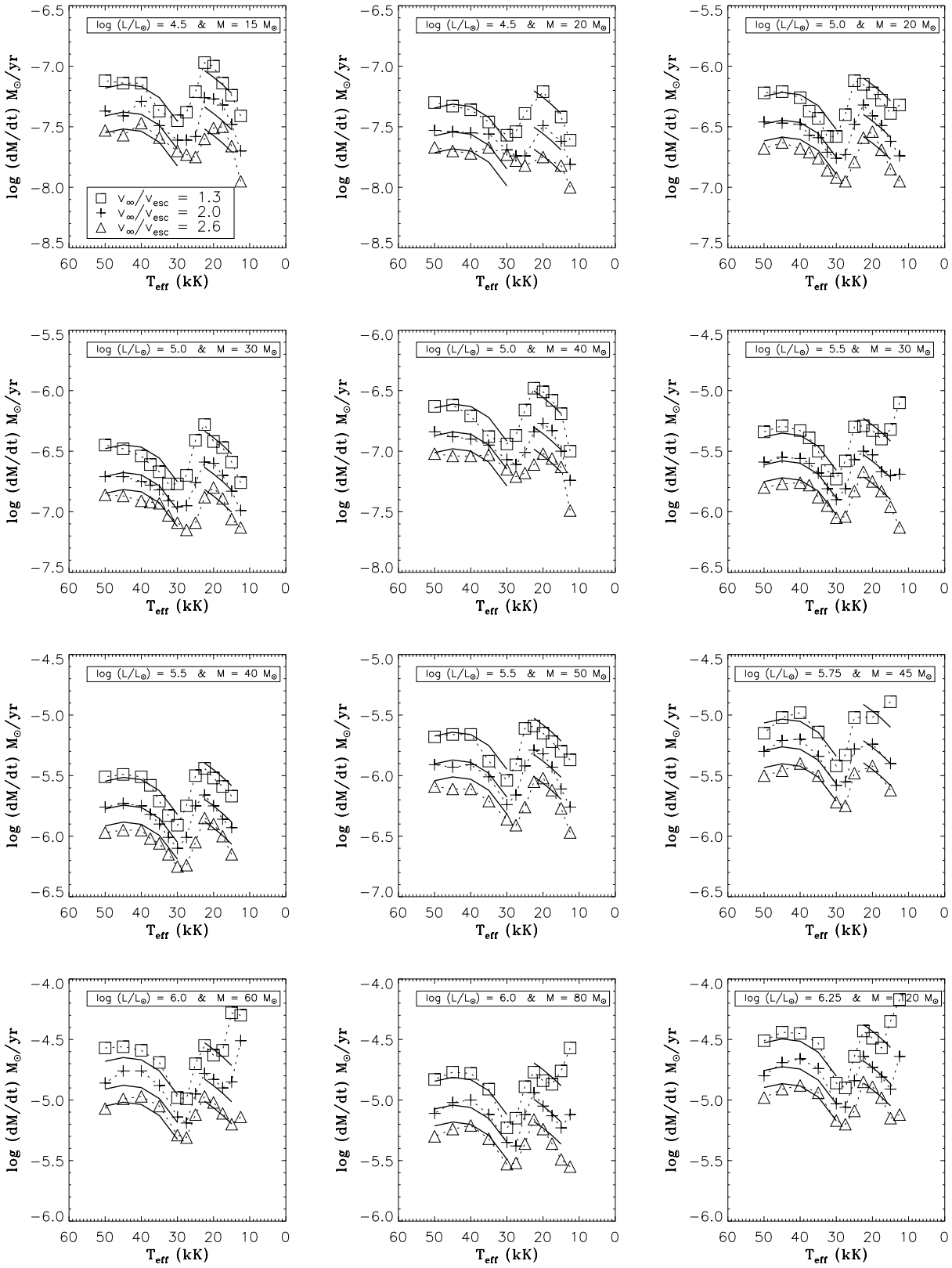

Fig. 2. The calculated mass-loss rates $\dot{M}$ as a function of $T_{\rm eff}$ for the grid of 12 (L_*, M_*) series for three values of the ratio $v_\infty/v_{\rm esc}$. The values for $v_\infty/v_{\rm esc}$ are indicated in the lower part of the first panel. The stellar parameters L_* and M_* are indicated in the upper part of each panel. The thin dotted lines connect the calculated mass-loss rates. The thick solid lines indicate two multiple linear regression fits to the calculated values (see Sect. 5). Note that some of the panels seem to indicate that a more accurate fit may be possible. However, the fits have been derived by *multiple* linear regression methods and thus the thick solid lines show the mass loss as a function of more than just one parameter. All models were calculated for solar metallicities.

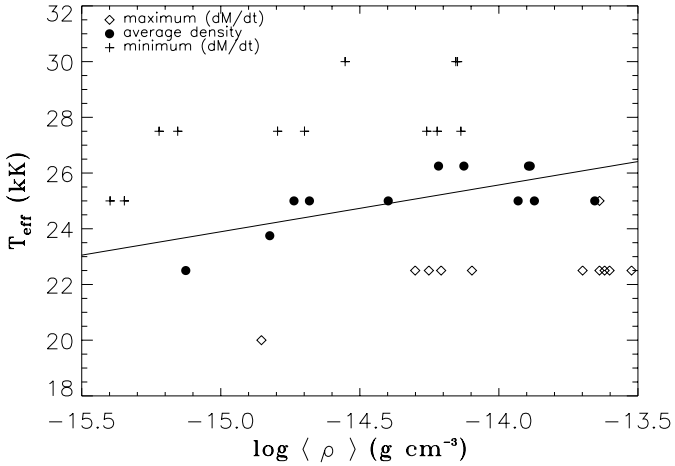

Fig. 3. Characteristic $\langle\rho\rangle$ and $T_{\rm eff}$ of the bi-stability jump around $T_{\rm eff}$ = 25 000 K. An explanation for the different symbols is given in the legend of the plot. The solid line represents a linear fit through the average jump parameters log $\langle\rho\rangle$ and $T_{\rm eff}$.

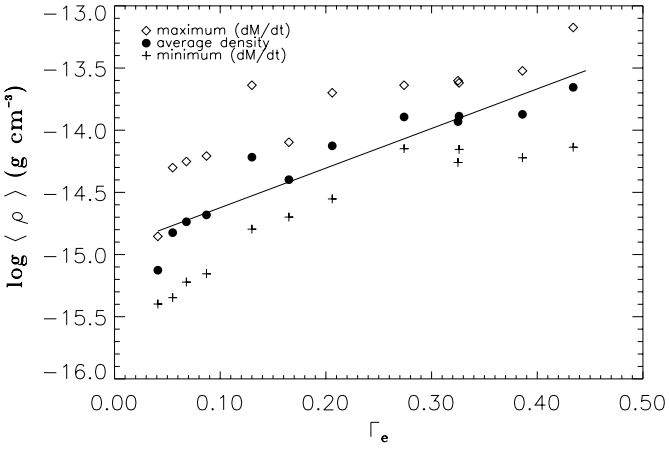

Fig. 4. Characteristic $\langle\rho\rangle$ at the bi-stability jump as a function of Γ_e. An explanation for the different symbols is given in the legend of the plot. The solid line indicates a linear fit through the average jump parameters for log $\langle\rho\rangle$.

to a larger density in the wind. Hence, the jump is expected to start at higher $T_{\rm eff}$ for smaller $v_\infty/v_{\rm esc}$. This behaviour for the position of $T_{\rm eff}$ of the jump is confirmed by all individual panels in Fig. 2. To understand the behaviour of the bi-stability jump as a function of the other stellar parameters, i.e. M_* and L_*, we will compare the wind characteristics of the 12 series of models around the bi-stability jump in some more detail.

First we define a characteristic wind density at 50% of the terminal velocity v_∞ of the wind: $\langle\rho\rangle$. For a standard velocity law with $\beta = 1$, this characteristic wind density is given by

$$\langle\rho\rangle \;=\; \frac{\dot{M}}{8\pi R_*^2 v_\infty} \qquad (3)$$

For all 12 series of models this characteristic density $\langle\rho\rangle$ is plotted vs. the effective temperature of the jump. This is done for both the minimum $\dot{M}$ (at the hot side of the jump) and the maximum $\dot{M}$ (at the cool side of the jump). Fig. 3 shows the location of the bi-stability jump in terms of $T_{\rm eff}$ as a function of $\langle\rho\rangle$. The characteristic densities and effective temperatures for the cool side of the jump are indicated with "diamond" signs and with "plus" signs for the hot side. As expected, for all 12 models the minimum $\dot{M}$ corresponds to a relatively low ρ and relatively high $T_{\rm eff}$, whereas the maximum $\dot{M}$ corresponds to a relatively high ρ, but low $T_{\rm eff}$. Note that the effective temperature at minimum and maximum mass loss is not a very smooth function of wind density. This is due to our choice of resolution in effective temperature of the grid. We have checked whether the obtained minima and maxima were indeed the extreme mass-loss values by calculating extra models at intermediate values of $T_{\rm eff}$. The minimum and maximum $\dot{M}$ values obtained with the initial grid resolution were found to be similar to those determined with a the finer resolution. We thus concluded that the initial resolution of the grid was justified.

The "filled circles" represent the average values of $T_{\rm eff}$ and $\langle\rho\rangle$ for the "jump" model for each (L_*, M_*) series. The "jump" model is a hypothetical model between the two models where $\dot{M}$ is maximal and minimal. The solid line indicates the best linear fit through these averages. The relation between the jump temperature (in kK) and log $\langle\rho\rangle$ is given by:

$$T_{\rm eff}^{\rm jump} \;=\; 49.1\,(\pm\,9.2) \;+\; 1.67\,(\pm\,0.64)\,\log\langle\rho\rangle \qquad (4)$$

The average temperature and density of the jump are given in Columns (5) and (6) of Table 2. Note that the range in $T_{\rm eff}^{\rm jump}$ is relatively small; all 12 series of models have jump temperatures in the range between $22.5 \lesssim T_{\rm eff} \lesssim 26$ kK.

Fig. 4 shows the behaviour of the characteristic density log $\langle\rho\rangle$ as a function of Γ_e. Again this is done for both the cool and hot side of the jump, and for the average between them. As expected, log $\langle\rho\rangle$ increases as Γ_e increases. Since the average characteristic wind density at the jump shows an almost linear dependence on Γ_e, a linear fit through the average densities is plotted. This is the solid line in Fig. 4. The relation between log $\langle\rho\rangle$ and Γ_e is given by:

$$\log\langle\rho\rangle \;=\; -\,14.94\,(\pm\,0.54) \;+\; 3.2\,(\pm\,2.2)\,\Gamma_e \qquad (5)$$

From the quantities L_* and M_* it is now possible to estimate log $\langle\rho\rangle$ using Eq. (5) and subsequently to predict $T_{\rm eff}^{\rm jump}$ using Eq. (4). Later on this will be used as a tool to connect two fitting formulae for the two ranges in $T_{\rm eff}$ at either side of the bi-stability jump (see Sect. 5).

3.3. $\dot{M}$ for supergiants in Range 2 (12 500 $\leq T_{\rm eff} \leq$ 22 500 K)

Fig. 2 shows that at effective temperatures $T_{\rm eff} \leq 22\,500$ K, $\dot{M}$ initially decreases. This is similar to the $\dot{M}$ behaviour in the $T_{\rm eff}$ range between 50 000 and 27 500 K. For some series (dependent on the adopted L_*/M_*) the mass loss decreases until our calculations end at $T_{\rm eff}$ = 12 500. For other series of L_* and M_*, the initial decrease suddenly switches to another *increase*. Vink et al. (1999) already anticipated that somewhere, at lower $T_{\rm eff}$, a recombination would occur from Fe III to II similar to the recombination from Fe IV to III at $\sim$ 25 000 K. Lamers

et al. (1995) already mentioned the possible existence of such a second bi-stability jump around $T_{\rm eff}$ = 10 000 K from their determinations of $v_\infty/v_{\rm esc}$, but the observational evidence for this second jump is still quite meagre.

3.4. $\dot{M}$ at the second bi-stability jump around 12 500 K

To understand the characteristics of the "second" bi-stability jump as a function of different stellar parameters (M_* and L_*), we have also studied the models around this second jump in some more detail.

Since our model grid is terminated at 12 500 K, it is not possible to determine the maximum $\dot{M}$ of the second bi-stability jump in a consistent way, similar to that of the first jump discussed in Sect. 3.2. Thus, it is not possible to determine the exact size of the second jump in $\dot{M}$. Neither is it possible to derive an accurate equation for the position of the second bi-stability jump in $T_{\rm eff}$ (as was done in Eq. 4 for the first jump around 25 000 K). Still, it is useful to determine a rough relationship between the position of the second jump in $T_{\rm eff}$ and the average $\log\langle\rho\rangle$ by investigating for each model at which temperature the mass-loss rate still decreases and for which models approaching the second bi-stability jump, the mass loss again increases.

The relation found between the temperature of the second bi-stability jump and $\log\langle\rho\rangle$ is determined by eye and is roughly given by:

$$T^{\rm jump2} \; = \; 100 \; + \; 6\,\log\langle\rho\rangle \qquad (6)$$

where $T^{\rm jump2}$ is in kK. From the quantities L_* and M_* it is again possible to estimate $\log\langle\rho\rangle$ using Eq. (5) and then to roughly predict $T^{\rm jump2}$ using Eq. (6). This formula will be used for our mass-loss recipe at the low temperature side (see Sect. 5).

4. The wind momentum

4.1. The wind efficiency number η

In this section, we present values for the wind efficiency number η for the different (L_*, M_*) series. η (sometimes called the wind performance number) describes the fraction of the momentum of the radiation that is transferred to the ions in the wind:

$$\dot{M}v_\infty \; = \; \eta\left(\frac{L_*}{c}\right) \qquad (7)$$

Fig. 5 shows the behaviour of η as a function of $T_{\rm eff}$ for the complete grid of models. Fig. 5 demonstrates that *η is not constant as a function of $T_{\rm eff}$*. The figure shows that when a star evolves redwards at constant luminosity (from high to low temperature) the momentum efficiency η initially decreases until the star approaches the bi-stability jump around 25 000 K, where the wind efficiency suddenly *increases* by a factor of two to three. Subsequently, below about 22 500 K, η decreases again and in some cases (again dependent on L_* and M_*) it eventually jumps again at the second bi-stability jump. This overall behaviour of η is similar to that of $\dot{M}$ as shown in Fig. 2.

In some of the panels of Fig. 5, i.e. in those cases where L_*/M_* is large, η exceeds the single scattering limit.

$$\eta \equiv \frac{\dot{M}v_\infty}{L_*/c} \geq 1 \qquad (8)$$

This occurs at $T_{\rm eff} \gtrsim 40\,000$ K and $\log(L_*/L_\odot) \gtrsim 6$. It suggests that already for high luminosity OB stars stellar winds cannot be treated in the *single scattering* formalism. The single-scattering limit which is definitely invalid for the optically thick winds of Wolf-Rayet type stars, is often assumed to be valid for the winds of "normal" supergiants. Here, however, we come to the conclusion that due to *multiple scattering*, η already exceeds unity for luminous, but "normal" OB supergiants, in case $\log(L/L_\odot) \gtrsim 6$. This was already suggested by Lamers & Leitherer (1993) on the basis of observations.

4.2. The importance of multiple scattering

Puls et al. (1996) proposed that the reason for the systematic discrepancy between the observed mass-loss rates and recent standard radiation driven wind models (Pauldrach et al. 1994) was caused by an inadequate treatment of multi-line effects in these wind models. To compare our new mass-loss predictions with the most sophisticated prior investigations, it is useful to briefly discuss the most important assumptions that are made in modelling the wind dynamics of OB-type stars. The following four basic choices must be made:

1. One may treat the photosphere and wind in a "core-halo" approximation, or one may not make this distinction and treat photosphere and wind in a "unified" way. This choice must be made twice, i.e. with respect to the calculation of the occupation numbers as well as with respect to the computation of the line force.
2. One may adopt a "single-line" approach, i.e. neglecting effects caused by overlapping lines, or one may follow an approach including "multi-line" effects.
3. One solves the rate equations for all relevant ions explicitly in non-LTE, or one adopts a "nebular type of approach" to calculate the ionization balance.
4. One solves the equation of motion self-consistently, or one derives the wind properties from a global energy argument.

Standard radiation driven wind models (CAK, Abbott 1982, Pauldrach et al. 1994) treat the momentum equation in a core-halo approach (1) adopting the single-line approximation (2). Various degrees of sophistication can be applied to determine the occupation numbers. The studies of Pauldrach et al. (1994) and Taresch et al. (1997) represent the current state-of-the-art, i.e. they treat all relevant ions explicitly in non-LTE (3) and solve the equation of motion self-consistently (4). Pauldrach et al. (1994) also use a unified method for the calculation of the occupation numbers, but a "core-halo"approach is applied with respect to the line force. Additionally, as line overlap is neglected in the method used by Pauldrach et al. (1994), these models can overestimate the line force as unattenuated photo-

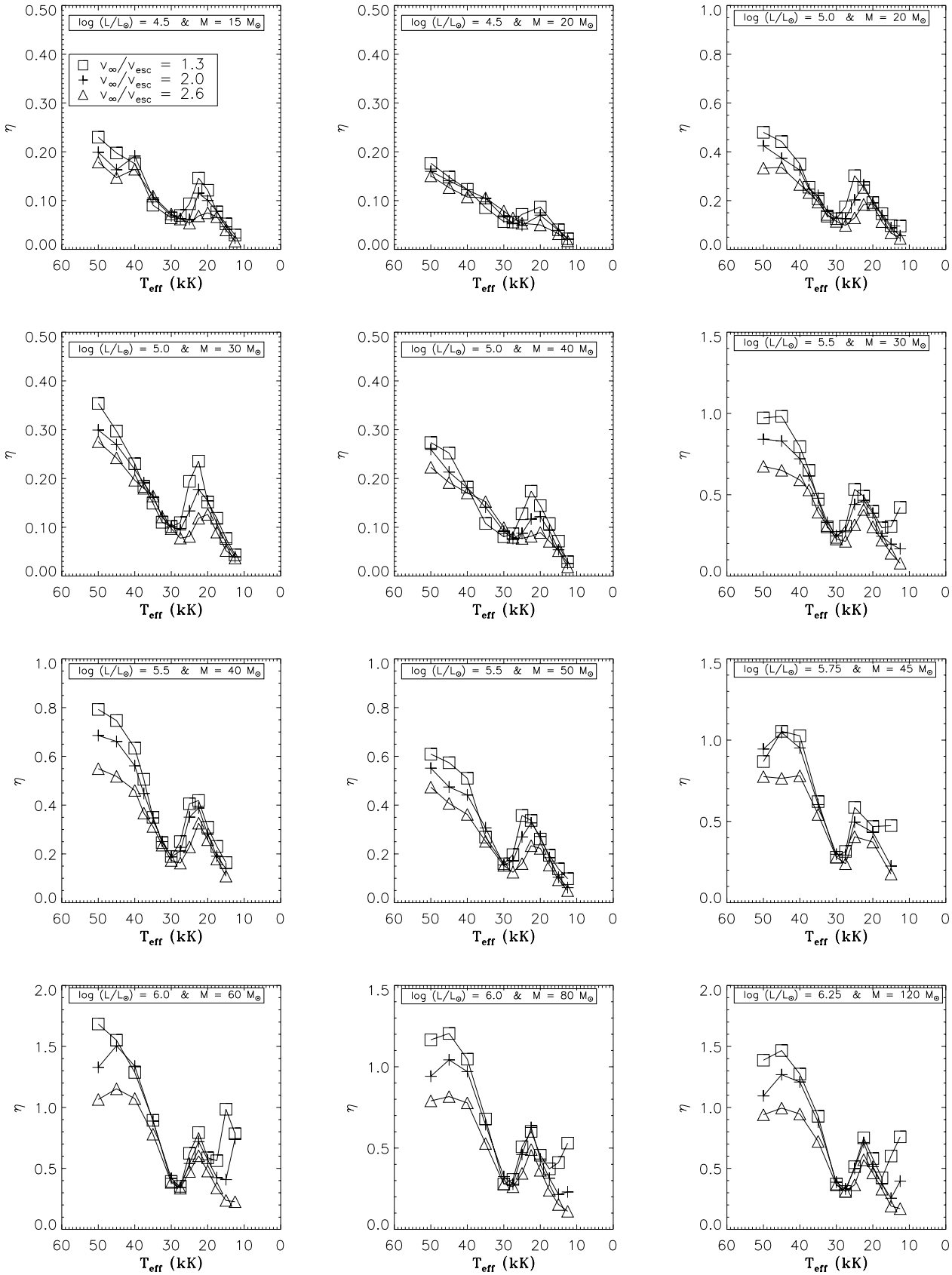

Fig. 5. The wind efficiency number η as a function of $T_{\rm eff}$ for the grid of 12 (L_*, M_*) series for three values of the ratio $v_\infty/v_{\rm esc}$. The values for $v_\infty/v_{\rm esc}$ are indicated in the legend of the first panel. The stellar parameters are indicated at the top of each panel. All models were calculated for solar metallicities.

spheric flux is offered to each line, which consequently may produce efficiency numbers larger than unity.

Puls (1987) found that for winds of relatively low density (say $\eta \lesssim 1/2$) the inclusion of multi-line effects leads to a reduction of wind momentum *compared to the standard model* due to backscattering and blocking of photons in the lower part of the wind. For winds of relatively high density (say $\eta \gtrsim 1$), such as the dense winds of Wolf-Rayet stars, the situation is likely to be reversed. Here momentum transfer from an extended diffuse field is expected to dominate over the effect of the attenuation of flux in the layers just above the photosphere. This could result in more mass loss compared to the standard radiation driven wind theory (Abbott & Lucy 1985, Springmann 1994). Wolf-Rayet and Of/WN stars profit from a layered ionization structure, which increases the number of lines that can be used for the driving and thus increasing the mass loss (Lucy & Abbott 1993, de Koter et al. 1997).

Our method differs in almost all aspects from that of Pauldrach et al. (1994). In our method, photosphere and wind are treated in a unified manner (1) and we properly take multi-scatterings into account with a Monte Carlo technique (2). On the other hand, we derive the level populations of the iron-group elements using (a sophisticated version of) the nebular approximation (3). Finally, we derive the mass loss from a global energy argument (4). This distinct difference of approach implies that a comparison between both methods is difficult. Still, we will address some of the differences in approach by focusing on a star with parameters representative for the O4I(f)-star ζ Puppis, which has been studied in detail by Abbott & Lucy (1985), Puls (1987), Pauldrach et al. (1994) and Puls et al. (1996).

We can test the difference between single scattering and multiple scattering by allowing photons to interact with a line only once. Fig. 6 show a comparison between the single- and multiple scattering case for three representative wind models at $T_{\rm eff}$ = 40,000 K. The model parameters are given in Table 3. For the often studied wind of the O supergiant ζ Puppis, which has a mass-loss rate of $\dot{M}^{\rm obs} = 5.9\times10^{-6} M_{\odot}{\rm yr}^{-1}$ (Puls et al. 1996), the observed efficiency number is about $\eta \simeq 0.6$, suggesting that the *real* efficiency of multiple vs. single scattering is a factor of about four for ζ Puppis (see Fig. 6). This is close to the findings of Abbott & Lucy (1985) who found an increase in $\dot{M}$ by a factor of 3.3 for the wind of ζ Puppis if multiple scattering was taken into account in a Monte Carlo simulation.

Note from the figure that at low wind densities, the single- and multiple scattering approach converge, as one would expect. For typical O-stars, which have $\eta \lesssim 0.5$, the mass loss will increase by up to a factor of two when multiple scattering is properly included. The Wolf-Rayet stars, located at the extreme high wind density side, and which in some cases have observed efficiency numbers of factors 10 or even higher, may benefit by factors of up to ~ 50.

The reason why Puls (1987) found a reduced mass loss for ζ Puppis when comparing the single-line approach with the multi-line approach is because the single-line approach (which is *not* the same as the single scattering process) overestimates the line force at the base of the wind, where the mass loss is fixed. However, a similar relative behaviour is *not* found when we compare the predicted single-line mass loss $\dot{M} = 5.1 \times 10^{-6} M_{\odot}{\rm yr}^{-1}$ of Pauldrach et al. (1994) with the value of $\dot{M} = 8.6 \times 10^{-6} M_{\odot}{\rm yr}^{-1}$ derived from our fitting formula based on multiple scattering models. It is not possible to exactly pinpoint the cause of this difference, but it is likely to be related to differences in our multi-line treatment and that of Puls (1987). Contrary to Puls (and also contrary to Abbott & Lucy 1985), we do not adopt the core-halo approximation. The formation region of the strong driving lines extends from the photosphere out to the base of the wind. If one assumes an input photospheric spectrum representative of the emergent ultraviolet spectrum as in a core-halo approach, one may overestimate the blocking in the subsonic wind regime which results in a lower mass loss.

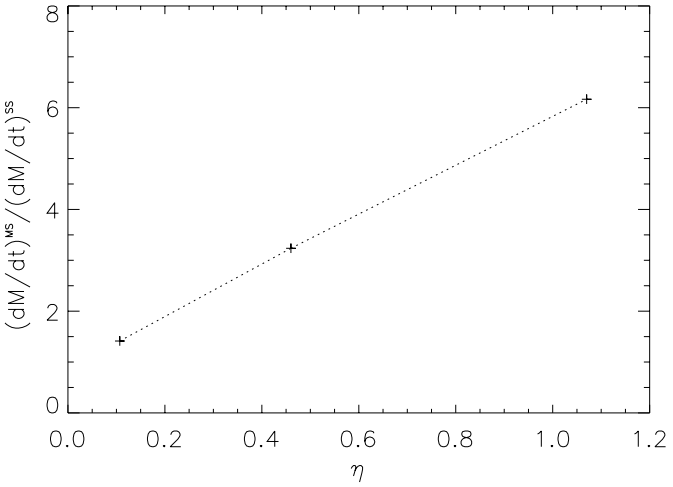

Fig. 6. The efficiency of multiple-scattering for a range of wind densities. MS refers to multiple-scattering, and SS refers to single-scattering.

Table 3. The relative importance of multiple (MS) vs. single scattering (SS) for a wind model at $T_{\rm eff} = 40\,000$ K.

$\Gamma_{\rm e}$	$\log L_*$ $(L_\odot)$	M_* $(M_\odot)$	$\eta^{\rm MS}$	$\log \dot{M}^{\rm SS}$	$\log \dot{M}^{\rm MS}$	$\frac{\dot{M}^{\rm MS}}{\dot{M}^{\rm SS}}$
0.041	4.5	20	0.107	-7.87	-7.72	1.41
0.206	5.5	40	0.460	-6.46	-5.95	3.24
0.434	6.0	60	1.07	-5.76	-4.97	6.17

4.3. The modified wind momentum Π

Kudritzki et al. (1995) have defined the Wind momentum Luminosity Relation (WLR):

$$\Pi \equiv \dot{M}\, v_\infty\, R_*^{0.5} \propto L_*^x \qquad (9)$$

where Π (or $\dot{M} v_\infty R_*^{0.5}$) is called the "modified wind momentum". Observations of $\dot{M}$ and v_∞ of O supergiants have shown that $\log \Pi$ is proportional to $\log L_*$ (see e.g. Puls et al. 1996). The WLR may in principle be used as a tool to derive distances to galaxies (see Kudritzki et al. 1995).

In the theory of line driven winds, the reciprocal value of x equals (Puls et al. 1996):

$$1/x = \alpha_{\rm eff} = \alpha - \delta \quad (10)$$

Here α and δ are force multiplier parameters, describing the radiative line acceleration $g_{\rm line}$ through the stellar wind:

$$g_{\rm line} \propto \left(\frac{1}{\rho}\frac{dv}{dr}\right)^{\alpha}\left(\frac{n_{\rm e}}{W}\right)^{\delta} \quad (11)$$

where $n_{\rm e}$ is the electron density and W is the dilution factor. α corresponds to the power law exponent of the line strength distribution function controlling the relative number of strong to weak lines. If only strong (weak) lines contribute to the line acceleration force, then α = 1 (0). The predicted value of α is about 0.6. The parameter δ describes the ionization balance of the wind. Values for this parameter are usually between 0.0 and 0.1. For a detailed discussion of the parameterisation of the line acceleration, see e.g. CAK, Abbott (1982) and Kudritzki et al. (1989).

The important point to note here is that possible changes in the slope x as a function of effective temperature reflect the fact that the stellar winds are driven by different sets of ions, i.e. lines of different ions. Fig. 5 shows that around the bi-stability jump at $T_{\rm eff} \simeq 25\,000$ K, η *increases* for decreasing $T_{\rm eff}$. This implies that one does not necessarily expect a universal WLR over the complete spectral range of O, B and A stars, nor does one expect a constant value of $\alpha_{\rm eff}$ or x for different spectral types.

5. Mass loss recipe

In this section we present a theoretical mass loss formula for OB stars over the full range in $T_{\rm eff}$ between 50 000 and 12 500 K. The mass-loss rate as a function of four basic parameters will be provided. These parameters are the stellar mass and luminosity, effective temperature and terminal velocity of the wind. To obtain a mass-loss recipe, we have derived interpolation formulae from the grid of $\dot{M}$ calculations presented in Sect. 3. The fitting procedure was performed using multiple linear regression methods to derive dependence coefficients. We have applied this method for the two ranges in $T_{\rm eff}$ separately. The first range is roughly the range for the O-type stars between $T_{\rm eff}$ = 50 000 and 30 000 K. The second range is between $T_{\rm eff}$ = 22 500 and 15 000 K, which is roughly the range for the B-type supergiants. The two relations are connected at the bi-stability jump. We have already derived the jump parameters for different series of models in Sect. 3, so we have knowledge about the position of the jump in $T_{\rm eff}$ as a function of stellar parameters. This will be applied in the determination of mass loss for stars with temperatures around the bi-stability jump.

5.1. Range 1 (30 000 $\leq T_{\rm eff} \leq$ 50 000 K)

The first range (roughly the range of the O-type stars) is taken from $T_{\rm eff}$ between 50 000 K and 30 000 K. In this range the step size in effective temperature equals 5 000 K. So, for the first range we have five grid points in $T_{\rm eff}$. Five times 12 series of (L_*, M_*), together with three ratios of $(v_\infty/v_{\rm esc})$ yields a total of 180 points in $\dot{M}$ for the first range. We have found that for the dependence of $\dot{M}$ on $T_{\rm eff}$, the fit improved if a second order term $(\log T_{\rm eff})^2$ was taken into account. In fact, this is obvious from the shapes of the plots in the panels of Fig. 2. The best fit that was found by multiple linear regression is:

$$\begin{aligned}\log \dot{M} = & -6.697\,(\pm0.061)\\ & +2.194\,(\pm0.021)\log(L_*/10^5)\\ & -1.313\,(\pm0.046)\log(M_*/30)\\ & -1.226\,(\pm0.037)\log\left(\frac{v_\infty/v_{\rm esc}}{2.0}\right)\\ & +0.933\,(\pm0.064)\log(T_{\rm eff}/40000)\\ & -10.92\,(\pm0.90)\,\{\log(T_{\rm eff}/40000)\}^2\end{aligned}$$

$$\text{for } 27\,500 < T_{\rm eff} \leq 50\,000\text{K} \quad (12)$$

where $\dot{M}$ is in $M_\odot$ yr^{-1}, L_* and M_* are in solar units and $T_{\rm eff}$ is in Kelvin. Note that M_* is the stellar mass *not* corrected for electron scattering. In this range $v_\infty/v_{\rm esc}$ = 2.6. Eq. 12 predicts the calculated mass-loss rates of the 180 models with a root-mean-square (rms) accuracy of 0.061 dex. The fits for the various (L_*, M_*) series are indicated with the thick lines in the panels of Fig. 2. Note that some of the panels in Fig. 2 seem to indicate that a more accurate fit might have been possible. However, Eq. (12) is derived by *multiple* linear regression methods and thus it provides the mass loss as a function of more than just one parameter.

5.2. Range 2 (15 000 $\leq T_{\rm eff} \leq$ 22 500 K)

The second range (roughly the range of the B-type supergiants) is taken from $T_{\rm eff}$ between 22 500 and 15 000 K. In this range the step size in effective temperature equals 2 500 K. For this range, there are four grid points in $T_{\rm eff}$. Four times 12 series of (L_*, M_*), together with three ratios of $(v_\infty/v_{\rm esc})$ yields a total of 144 points in $\dot{M}$. In this range the fit did not improve if a second order term in effective temperature was taken into account, so this was not done. The best fit that was found by multiple linear regression for the second range is:

$$\begin{aligned}\log \dot{M} = & -6.688\,(\pm0.080)\\ & +2.210\,(\pm0.031)\log(L_*/10^5)\\ & -1.339\,(\pm0.068)\log(M_*/30)\\ & -1.601\,(\pm0.055)\log\left(\frac{v_\infty/v_{\rm esc}}{2.0}\right)\\ & +1.07\,(\pm0.10)\log(T_{\rm eff}/20000)\end{aligned}$$

$$\text{for } 12\,500 < T_{\rm eff} \leq 22\,500\text{K} \quad (13)$$

where again $\dot{M}$ is in $M_\odot$ yr^{-1}, L_* and M_* are in solar units and $T_{\rm eff}$ is in Kelvin. In this range $v_\infty/v_{\rm esc}$ = 1.3. The fitting formula is also indicated by solid lines in the panels of Fig. 2.

Eq. 13 predicts the calculated mass-loss rates of the 144 models for this $T_{\rm eff}$ range with an rms accuracy of 0.080 dex. For this second range (12 500 $< T_{\rm eff} \leq$ 22 500 K) the fit is slightly less good than for the first $T_{\rm eff}$ range. This is due to the presence of the second bi-stability jump which already appears in some (L_*/M_*) cases, as was shown in Fig. 2. If those models that do show the *second* bi-stability jump, i.e. stars with high Γ_e, are omitted from the sample, the accuracy improves to $\simeq 0.06$ dex. In all cases the rms is $\lesssim 0.08$ dex in $\log \dot{M}$, which implies that the fitting formulae yield good representations of the actual model calculations.

We are aware of the fact that there could be systematic errors in our approach, since we have made assumptions in our modelling. For a discussion of these assumptions, see Vink et al. (1999). Whether there are still systematic errors between the observed mass-loss rates and these new predictions of radiation-driven wind theory, will be investigated in Sect. 6.

5.3. The complete mass-loss recipe

For stars with effective temperatures higher than 27 500 K, one should apply the mass-loss formula for the first range (Eq. 12); for stars with $T_{\rm eff}$ lower than 22 500 K the formula for the second range (Eq. 13) is to be used. In the range between 22 500 and 27 500 K, it is not a priori known which formula to apply. This due to the presence of the bi-stability jump. Nevertheless, it is possible to retrieve a reliable mass-loss prediction by using Eqs. 4 and 5 as a tool to determine the position of the jump in $T_{\rm eff}$.

In predicting the mass-loss rate of stars close to the bi-stability jump, one should preferentially use the *observed* $v_\infty/v_{\rm esc}$ value to determine the position with respect to the jump. This is a better approach than to use the tools from Eqs. 4 and 5 to determine the position of the jump. The reason is that errors in the basic stellar parameters may accidently place the star at the wrong side of the jump. A computer routine to calculate mass loss as a function of input parameters is available either upon request or at the following url: www.astro.uu.nl/∼jvink/.

If v_∞ is not available, as is the case for evolutionary calculations, one should adopt the ratio $v_\infty/v_{\rm esc}$ = 2.6 for the hot side of the jump and $v_\infty/v_{\rm esc}$ = 1.3 for the cool side of the jump, in agreement with the analysis by Lamers et al. (1995). Note that the exact $T_{\rm eff}$ of the jump is not expected to have a significant effect on evolutionary tracks calculated with this new mass-loss description, since the most luminous stars spend only a relatively short time around $T_{\rm eff} \simeq$ 25 000 K during their evolution.

Since our calculations were terminated at 12 500 K, we are not able to determine the size and the position of the second bi-stability jump. Predicting the mass-loss behaviour below this second jump would therefore be speculative. Yet, for evolutionary tracks the mass loss below 12 500 K is an important ingredient in the evolutionary calculations. We roughly estimate from our grid calculations that for a *constant* ratio of $v_\infty/v_{\rm esc}$ the increase in $\dot{M}$ around 12 500 is about a factor of two, similar to that found for the first jump near 25 000 K. Furthermore, observations by Lamers et al. (1995) indicate that for stars around 10 000 K, $v_\infty/v_{\rm esc}$ drops again by a factor of two from $v_\infty/v_{\rm esc} \simeq$ 1.3 to about 0.7. It is therefore plausible to expect that the size in $\dot{M}$ of the second jump is comparable to the size of the first jump. So, $\Delta\dot{M}$ of the second jump is expected to be a factor of five also. We argue that this second jump should also be considered in evolutionary calculations and suggest Eq. (13) could be used for effective temperatures below the second jump when the constant in Eq. (13) is increased by a factor of five (or $\log \Delta\dot{M}$ = 0.70) to a value of -5.99. The mass-loss recipe can be applied for evolutionary calculations until the point in the HRD where line driven winds become inefficient and where probably another mass-loss mechanism switches on for the cooler supergiants (see Achmad et al. 1997). We suggest that in the temperature range below the second jump $v_\infty/v_{\rm esc}$ = 0.7 is adopted.

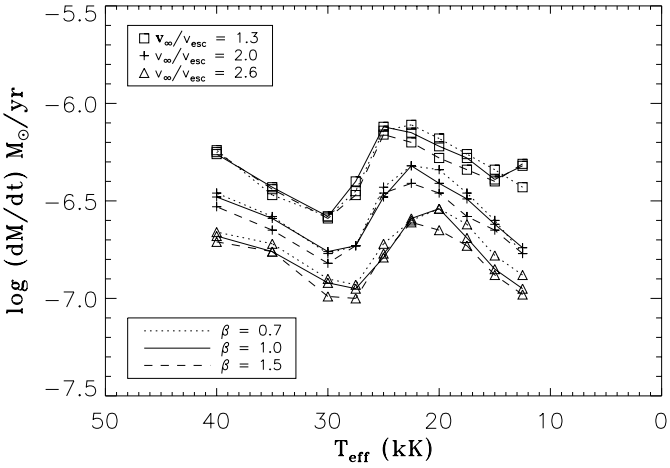

Fig. 7. Dependence of $\dot{M}$ on the shape of the velocity law, for three values of β = 0.7, 1.0 and 1.5, as is indicated in the lower left corner of the plot. The values for $v_\infty/v_{\rm esc}$ are indicated in the upper left corner of the plot. For other stellar parameters, see text.

5.4. The dependence of $\dot{M}$ on the steepness of the velocity law β

To test the sensitivity of our predictions of mass-loss rates on different shapes of the velocity law, we have calculated series of models for β = 0.7, 1.0 and 1.5. This is a reasonable range for OB stars, see Groenewegen & Lamers 1989; Puls et al. 1996). The adopted stellar parameters for this test are $L_* = 10^5\ L_\odot$ and $M_* = 20\ M_\odot$. We have calculated $\dot{M}$ for all of the above β values for wind models with the three values $v_\infty/v_{\rm esc}$ = 2.6, 2.0 and 1.3.

From the results shown in Fig. 7 we derived for the dependence of $\dot{M}$ on the adopted value of β:

$$\log \dot{M} = C \ + \ 0.112\ (\pm 0.048)\ \log(\beta/1.0) \qquad (14)$$

where C is a constant. This relation is valid for the range between β = 0.7–1.5. Since the dependence on this parameter is significantly smaller than that on the other parameters, L_*, M_*, $T_{\rm eff}$ and $v_\infty/v_{\rm esc}$, as was found in Eqs. 12 and 13, we have omitted the β dependence from the mass loss recipe. We have just presented the β dependence in this section for the sake of

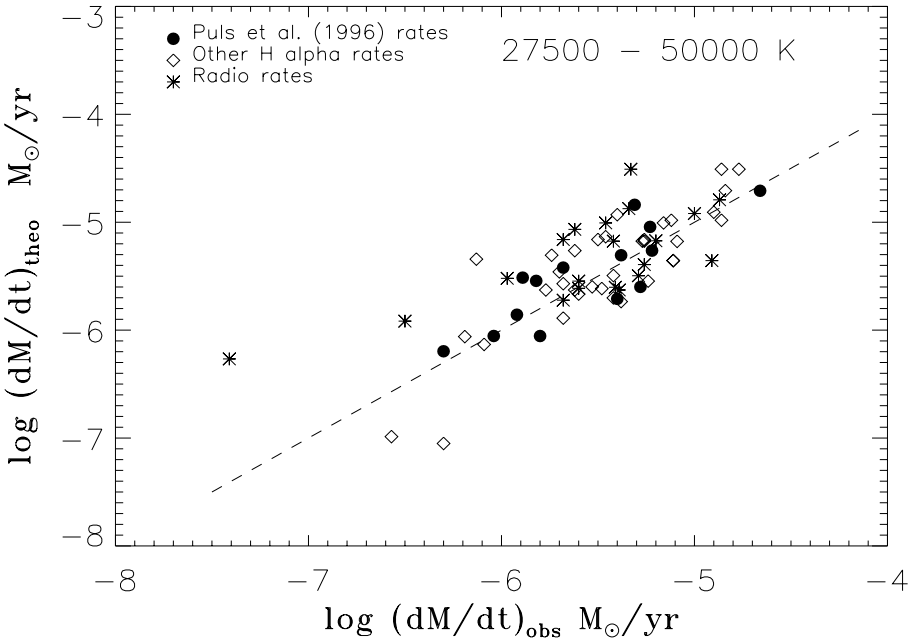

Fig. 8. Comparison between theoretical and observational $\dot{M}$ (both radio data and Hα) for the O stars. The Puls et al. (1996) Hα rates; Hα rates from other determinations, and radio mass-loss rates are indicated with different symbols. The dashed line is a one-to-one relation.

completeness, but we can conclude that the predicted mass-loss rates are only marginally sensitive to the *shape* of the adopted velocity law. One could argue that a β dependence on $\dot{M}$ could be of significance for more extreme series of models. This was tested, but it turned out that for the high Γ_e series, the β dependence is also insignificant, i.e. deviations of predicted $\dot{M}$ are less than $\Delta\dot{M} \lesssim 0.03$ dex. This shows that we can safely omit the β dependence on $\dot{M}$ in the mass-loss recipe for the O and B stars.

6. Comparison between theoretical and observational $\dot{M}$

6.1. $\dot{M}$ comparison for Range 1 (27 500 $< T_{\rm eff} \leq$ 50 000 K)

An extended compilation of observed mass-loss rates of early-type OBA stars is obtained by Lamers et al. (2000; in preparation). Since both the ultraviolet and the infrared method do not yet yield reliable rates, only mass-loss rates based on radio free-free emission and emission of Hα have been considered. The Hα mass-loss rates and their stellar parameters are from: Herrero et al. (2000); Kudritzki et al. (1999); Lamers & Leitherer (1993) (these Hα equivalent width values are corrected with the curve of growth method from Puls et al. 1996); Puls et al. (1996); Scuderi et al. (1992), Scuderi (1994), and Scuderi & Panagia (2000). The radio rates are from the compilation of Lamers & Leitherer (1993); from Leitherer et al. (1995) and Scuderi et al. (1998). The observed terminal velocities are from the same papers. These were mainly determined from P Cygni profiles. The stellar masses are derived from evolutionary tracks of Meynet et al. (1994). For a critical discussion of the observed mass-loss rates and for the selection of the most reliable data, see Lamers et al. (in preparation).

For all these stars with known observational mass-loss rates and stellar parameters, we have determined theoretical $\dot{M}$ values with the mass-loss recipe that was derived in Sect. 5. A star-to-star-comparison between these predicted mass-loss rates and those derived from observations is presented in Fig. 8. In this plot only the stars above the bi-stability jump (where $T_{\rm eff} \geq$ 27 500 K) are included. The mass-loss rates from Puls et al. (1996) are indicated with a different symbol (filled circle), because these are obtained from a homogeneous set, and are analyzed with the most sophisticated wind models. Note that the outlier at log $\dot{M}_{\rm obs} \simeq$ - 7.4 is the star ζ Oph (HD 149757) for which Lamers & Leitherer (1993) reported that the mass-loss rate is uncertain.

The errors in Fig. 8 can be due to several effects. There is an error in the theoretical fitting formula, though this error is only 0.061 dex (see Sect. 5.1). There could also be systematic errors due to assumptions in the modelling. Furthermore, there could be systematic errors in the mass-loss determinations from observations. Such systematic effects may for instance occur if the clumping factor in the wind changes with distance to the central star. This because the Hα and radio emission originate from distinctly different regions in the stellar wind. However, Lamers & Leitherer (1993) have shown that for a significant sample of O stars there is good agreement between the radio and the Hα mass-loss rates.

The random errors in the observational mass-loss rates are due to uncertainties in the stellar parameters and in the mass-loss determinations. We tentatively estimate the intrinsic errors in the observed mass-loss rates from the radio and Hα method to be on the order of 0.2–0.3 dex (see Lamers et al. in preparation). This means that for a star-by-star comparison between observations and theory one would expect a scatter around the mean which is a combination of the theoretical and observed uncertainties. This error is on the order of 0.3 dex. The scatter between observational and theoretical mass-loss rates for the O stars from Fig. 8 that was actually derived, equals 0.33 dex ($1\,\sigma$) for the complete set and is 0.24 dex for the Puls et al. set. This

is an expected scatter and it implies that *we do not find a systematic discrepancy between observations and our predictions for the O star mass-loss rates*.

Contrary to earlier comparisons between observations and theory where systematic discrepancies have been reported (see Lamers & Leitherer 1993, Puls et al. 1996), here we find that there is agreement between our predictions and the mass-loss rates derived from observations for the O-type stars. The essential difference between previous studies and the present one is that in our treatment of the theory of line driven winds, we consistently take into account effects of "multiple-scattering" in the transfer of momentum from the radiation field to the wind. We find systematic agreement between observed and theoretical mass-loss rates for a *large sample* of O stars. This result implies that physical effects that were not incorporated in our models, such as magnetic fields and stellar rotation, is not expected to influence the mass-loss rates of O stars significantly.

6.2. Modified wind momentum comparison for Range 1 ($27\,500 < T_{\rm eff} \leq 50\,000$ K)

Instead of comparing just the mass-loss rates it is useful to compare (modified) wind momenta derived from observations and theory. In earlier studies, e.g. Lamers & Leitherer (1993), and Puls et al. (1996), wind momenta have been plotted versus the wind efficiency number η. Comparisons between observed and theoretical wind momenta as a function of η could yield important information about the origin of the systematic discrepancy between theory and observations. However, since these two quantities (wind momentum and wind efficiency number) both contain the mass-loss rate, they are not independent. Therefore, no such comparison is made here. Instead, the wind momenta are plotted versus the stellar luminosity, to compare the observational and theoretical WLR.

We divide the $T_{\rm eff}$ range into two parts. First, we examine the wind momenta for stars where $T_{\rm eff} \geq 27\,500$ K, later on we will also compare the cooler stars. Fig. 9 shows the modified wind momentum as a function of stellar luminosity for the sample of stars with known observational mass-loss rates. The upper panel shows these modified wind momentum values for the theoretical mass-loss rates and a linear best fit through these theoretical data (dotted line). Note that the "theoretical" WLR only contains the theoretical $\dot{M}$, the included values for v_∞ and R_* were taken from observations. The theoretical WLR is:

$$\begin{aligned} \Pi^{\rm theory} \;=\; & -12.12\,(\pm 0.26) \\ & +\;1.826\,(\pm 0.044)\,\log(L/L_\odot) \end{aligned}$$

$$\text{for } T_{\rm eff} \;\geq\; 27\,500 \text{ K} \qquad (15)$$

Since the slope of the WLR of Eq. (15) has a slope of $x = 1.826$, the derived theoretical value for $\alpha_{\rm eff}$ (Eq. 10) that follows, is:

$$\alpha_{\rm eff} \;=\; \frac{1}{x} \;=\; 0.548 \qquad (16)$$

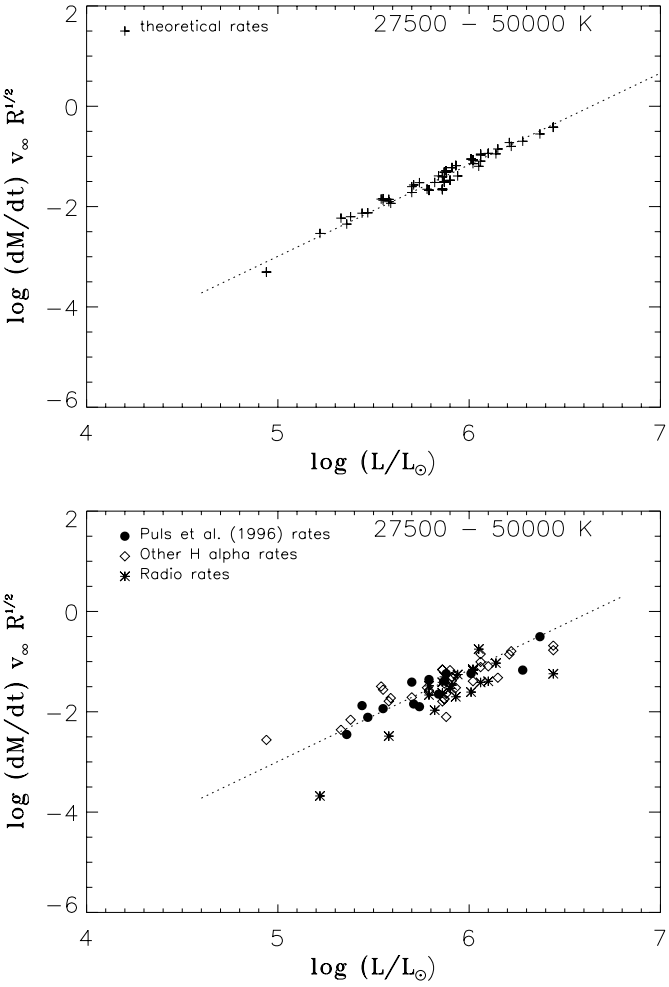

Fig. 9. Upper panel: The theoretical modified wind momentum expressed in $M_\odot/{\rm yr\,km\,s^{-1}}\;{R_\odot}^{0.5}$ for the stars in the first $T_{\rm eff}$ range ($27\,500 < T_{\rm eff} \leq 50\,000$ K). The dotted line indicates the best linear fit. Lower panel: The observational modified wind momentum for these stars. The dotted line indicates the same theoretical linear fit, as in the upper panel.

This corresponds well to predicted values of the force multiplier parameter ($\alpha \simeq 0.66$ and $\delta \simeq 0.10$, see e.g. Pauldrach et al. 1994).

The lower panel of Fig. 9 shows that both the WLR for the Puls et al. (1996) data and that for the other methods/authors, follow the same relationship, both in agreement with the theoretical WLR. The dotted line is again the theoretical best linear fit. We conclude that for the range of the O stars, there is good agreement between theoretical wind momenta and those determined from observations. The scatter between theoretical and observational modified wind momenta is only 0.06 (1 σ).

The good agreement between the observational and theoretical wind momenta adds support to the possibility to derive distances to luminous, hot stars in extragalactic stellar systems using the WLR. In practice the technique may be hampered by e.g. the fact that O stars are mostly seen in stellar clusters and cannot be spatially resolved in distant stellar systems. This is

one of the reasons why the visually brighter B-type and especially the A-type supergiants located in the field are expected to be better candidates in actually using the WLR as a distance indicator (see Kudritzki et al. 1999).

Comparison between the theoretical and observational WLR for the winds of B and A type supergiants is thus essential to investigate whether the slope of the WLR is the same for different spectral ranges. This is not expected, since the winds of different spectral types are driven by lines of different ions (see Vink et al. 1999; Puls et al. 2000).

6.3. Modified wind momentum comparison for Range 2 (12 500 $\leq T_{\rm eff} \leq$ 22 500 K)

Fig. 10 shows the modified wind momentum as a function of luminosity for both theory and observations for the stars in the second range (12 500 $\leq T_{\rm eff} \leq$ 22 500 K). A best fit through the theoretically derived WLR is indicated with a dotted line in both panels. The theoretical WLR for this $T_{\rm eff}$ range is:

$$\Pi^{\rm theory} = -12.28\,(\pm 0.23) + 1.914\,(\pm 0.043)\log(L/L_\odot)$$

$$\text{for } 12\,500 \leq T_{\rm eff} \leq 22\,500 \text{ K} \qquad (17)$$

Since the slope of the WLR for this range is slightly higher than that for the O star range, the predicted value for $\alpha_{\rm eff}$ is somewhat lower (see Sect. 4.3), namely:

$$\alpha_{\rm eff} = \frac{1}{x} = 0.522 \qquad (18)$$

The lower panel of Fig. 10 indicates the observed modified wind momenta (the dotted line contains the *theoretical* mass-loss rates). For this second $T_{\rm eff}$ range (12 500 $\leq T_{\rm eff} \leq$ 22 500 K) the plot in the lower panel reveals a large scatter in the observed data.

Comparison of these observations with our predictions shows that within the subset of radio mass-loss rates there does not appear to be a systematic discrepancy. Also, those Hα profiles which are fully in emission (the filled symbols in the lower panel of Fig. 10), i.e. the profiles that within the Hα method most likely provide the most reliable mass-loss rates, do not show a systematic difference with the radio rates. The picture becomes different for stars that show Hα to be P Cygni shaped (grey symbols in lower panel of Fig. 10) or fully in absorption (open symbols). Although the measurements of Scuderi (1994,2000) remain reasonably consistent, those by Kudritzki et al. (1999) are discrepant in that at log $L/L_\odot \simeq 5.8$ these values start to diverge from the other observed rates, such that below log $L/L_\odot \simeq 5.6$ a systematic difference of about a factor of 30 results between different sets of observed mass-loss rates.

An investigation of the origin of these systematic differences in observed B star wind momenta is beyond the scope of this paper. We will address this issue in a separate study (Lamers et al., in preparation). Here we just note that the large scatter in the observed Hα data implies that there is either a dichotomy

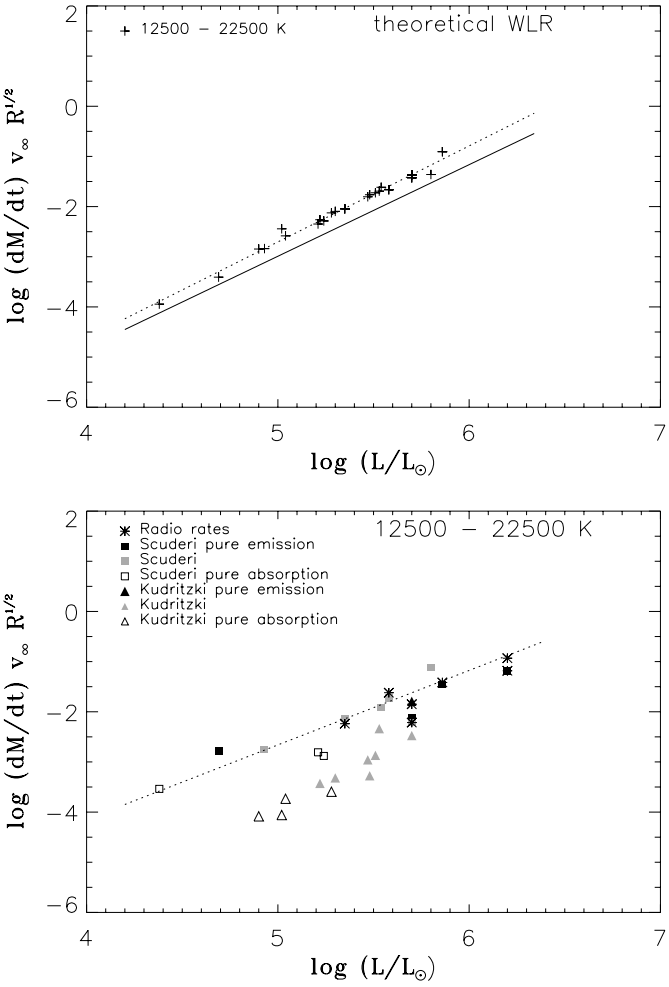

Fig. 10. Upper panel: The *theoretical* modified wind momentum expressed in $M_\odot/{\rm yr\,km\,s^{-1}}\,{R_\odot}^{0.5}$ for the second range (12 500 $\leq T_{\rm eff} \leq$ 22 500 K). The *dotted* line indicates the best linear fit for this range. The solid line indicates the theoretical WLR for stars in the range 27 500 $< T_{\rm eff} \leq$ 50 000 K. Lower panel: The *observational* modified wind momentum for stars in this $T_{\rm eff}$ range (12 500 $\leq T_{\rm eff} \leq$ 22 500 K). The different sources of the observations are indicated in the upper left corner. The dotted line again indicates the *theoretical* linear fit for the stars in the second range (12 500 $\leq T_{\rm eff} \leq$ 22 500 K).

in the wind-momenta of B-stars (as suggested by Kudritzki et al. 1999) or that there exist systematic errors in the mass-loss determinations from Hα for B stars.

The systematic discrepancies for the observed B star wind momenta imply that we cannot currently compare our predictions with observed data in the most meaningful way, since the data are not consistent and thus a fair comparison with our predictions cannot be conclusive. In addition, it may be meaningful to further investigate the validity of assumptions in our method of predicting the mass-loss rates of B-type stars (see e.g. Owocki & Puls 1999). Still, we note that the most reliable rates (from radio and pure Hα emission profiles) appear to be consistent with our predictions.

The upper panel of Fig. 10 reveals that most of the models in the second $T_{\rm eff}$ range (12 500 $\leq T_{\rm eff} \leq$ 22 500 K) lie *above*

the theoretical fit for the models from the first $T_{\rm eff}$ range ($T_{\rm eff} \geq$ 27 500 K). This is due to the increase in the mass-loss rate at the bi-stability jump of a factor of five. The models with 12 500 $\leq T_{\rm eff} \leq$ 22 500 K are, however, only slightly above the fit for the O star models ($T_{\rm eff} \geq$ 27 500 K), as at the bi-stability jump the terminal velocity v_∞ drops by a factor of two.

7. Discussion

We have shown that our predictions of mass loss for O stars, using Monte Carlo simulations of energy loss during photon transport in non-LTE unified wind models, yields good agreement with the observed values. This demonstrates that an adequate treatment of "multiple scattering" in radiation-driven wind models resolves the discrepancy between observations and theory that had been reported earlier. The agreement between observed and theoretical wind momenta of O stars adds support to the method of deriving distances to distant stellar systems using the WLR.

The comparison between the predicted and observed values of the modified wind momentum Π for the B stars is not conclusive. A good comparison between the observations and our predictions for the B star regime needs to await an explanation of the discrepancies in the observed B star mass-loss rates. This issue will be addressed in a separate study.

Our models predict a jump in mass loss of about a factor of five around spectral type B1. An important point that supports this prediction is the following. Vink et al. (1999) have calculated the mass-loss rate and v_∞ for winds at both sides of the bi-stability jump in a self-consistent way for models with log(L/$L_\odot$) = 5.0 and M = 20 $M_\odot$. These self-consistent calculations showed a jump in $\dot{M}$ of a factor of five and a simultaneous drop in $v_\infty/v_{\rm esc}$ of a factor of two. This drop in $v_\infty/v_{\rm esc}$ has been *observed* (Lamers et al. 1995). This gives support to our prediction that the mass-loss rate at spectral type B1 increases by the predicted amount.

Since there is good agreement between observed mass-loss rates by different methods and the new theoretical mass-loss rates for the O-type stars, whereas there is inconsistency between the observed mass-loss rates from different authors for the B-type stars, this may point to the presence of systematic errors in mass-loss determinations from observations for B stars.

Because our predictions for the O stars agree with observations and our models also predict the bi-stability jump around spectral type B1, we believe that our theoretical mass-loss predictions are reliable and suggest they be used in new evolutionary calculations of massive stars.

8. Summary and conclusions

1. We have calculated a grid of wind models and mass-loss rates for a wide range of stellar parameters, corresponding to masses between 15 and 120 $M_\odot$.
2. We have derived two fitting formulae for the mass-loss rates in two ranges in $T_{\rm eff}$ at either side of the bi-stability jump around 25 000 K. A mass-loss recipe was derived that connects the two fitting formulae at the bi-stability jump.
3. There is good agreement between our mass-loss predictions that take *multiple scattering* into account, and the observations for the O stars. There is no systematic difference between predicted and observed mass-loss rates.
4. A comparison between observed and predicted wind momenta of O-type stars also shows there is good agreement. This adds support to the use of the WLR as a way to derive distances to luminous O stars in distant stellar systems.
5. For the observed mass-loss rates of B stars there is an inconsistency between rates derived by different authors and/or methods. One group of $\dot{M}$ determinations of B stars does follow the theoretical relationship, while another group does not. This lack of agreement between the observed mass-loss rates of B stars may point to systematic errors in the observed values.
6. Since our new theoretical mass-loss formalism is successful in explaining the observed mass-loss rates for O-type stars, as well as in predicting the location (in $T_{\rm eff}$) and size (in $v_\infty/v_{\rm esc}$) of the observed bi-stability jump, we believe that our predictions are reliable and suggest that our recipe be used in new evolutionary calculations for massive stars. A computer routine to calculate mass loss is available either upon request or at the following url: www.astro.uu.nl/$\sim$jvink/.

Acknowledgements. We thank the referee, Joachim Puls, for constructive comments that helped improve the paper. JV acknowledges financial support from the NWO Council for Physical Sciences. AdK acknowledges support from NWO Pionier grant 600-78-333 to L.B.F.M. Waters and from NWO Spinoza grant 08-0 to E.P.J. van den Heuvel.

References

Abbott D.C., 1982, ApJ 259, 282
Abbott D.C., Lucy L.B., 1985, ApJ 288, 679
Achmad L., Lamers H.J.G.L.M., Pasquini L., 1997, A&A 320, 196
Allen C.W., 1973, Astrophysical quantities. Athlone Press
Castor J.I., Abbott D.C., Klein R.I., 1975, ApJ 195, 157
Chiosi C., Maeder A., 1986, ARA&A 24, 329
de Koter A., Schmutz W., Lamers H.J.G.L.M., 1993, A&A 277, 561
de Koter A., Heap S.R., Hubeny I., 1997, ApJ 477, 792
Groenewegen M.A.T., Lamers H.J.G.L.M., 1989, A&AS 79, 359
Haser S., Lennon D.J., Kudritzki R.-P., 1995, A&A 295, 136
Herrero A., Puls J., Villamariz M.R., 2000, A&A 354, 193
Kudritzki R.-P., Pauldrach A.W.A., Puls J., Abbott D.C., 1989, AAP 219, 205
Kudritzki R.-P, Lennon D.J., Puls J., 1995, In: Walsh J.R., Danziger I.J. (eds.) Science with the VLT. Springer Verlag, p. 246
Kudritzki R.-P., Puls J., Lennon D.J., et al., 1999, A&A 350, 970
Lamers H.J.G.L.M., Leitherer C., 1993, ApJ 412, 771
Lamers H.J.G.L.M., Snow T.P., Lindholm D.M., 1995, ApJ 455, 269
Lamers H.J.G.L.M., Nugis T., Vink J.S., de Koter A., 2000, In: Lamers H.J.G.L.M., Sapar A. (eds.) Thermal and ionization aspects from hot stars. ASP Conf. Ser. 204, p. 395
Leitherer C., Chapman J., Korabalski B., 1995, ApJ 450, 289
Lucy L.B., Solomon P., 1970, ApJ 159, 879
Lucy L.B., Abbott D.C., 1993, ApJ 405, 738

Meynet G., Maeder A., Schaller G., Schearer D., Charbonel C., 1994, A&AS 103, 97
Owocki S.P., Puls J., 1999, ApJ 510, 355
Pauldrach A.W.A., Puls J., Kudritzki R.P., 1986, A&A 164, 86
Pauldrach A.W.A., Kudritzki R.P., Puls J., Butler K., Hunsinger J., 1994, A&A 283, 525
Puls J., 1987, A&A 184, 227
Puls J., Kudritzki R.P., Herrero A., et al., 1996, A&A 305, 171
Puls J., Springmann U., Lennon M., 2000, A&AS 141, 23
Schmutz W., 1991, In: Crivellari L., Hubeny I., Hummer D.G. (eds.) Stellar Atmospheres: Beyond Classical Models. NATO ASI Series C, Vol. 341, p. 191
Scuderi S., 1994, Properties of winds of early type stars. Thesis, Univ. of Catania
Scuderi S., Panagia N., 2000, In: Lamers H.J.G.L.M., Sapar A. (eds.) Thermal and ionization aspects from hot stars. ASP Conf. Ser. 204, p. 419
Scuderi S., Bonanno G., Di Benedetto R., Sparado D., Panagia N., 1992, A&A 392, 201
Scuderi S., Panagia N., Stanghellini C., Trigilio C., Umana C., 1998, A&A 332, 251
Springmann U., 1994, A&A 289, 505
Taresch G., Kudritzki R.P., Hurwit M., et al., 1997, A&A 321, 531
Vink J.S., de Koter A., Lamers H.J.G.L.M., 1999, A&A 350, 181